Science Advances

AAAS

advances.sciencemag.org/cgi/content/full/3/12/eaao3773/DC1

# Supplementary Materials for

## Quantum criticality in the spin-1/2 Heisenberg chain system copper pyrazine dinitrate

Oliver Breunig, Markus Garst, Andreas Klümper, Jens Rohrkamp, Mark M. Turnbull, Thomas Lorenz

Published 22 December 2017, *Sci. Adv.* **3**, eaao3773 (2017)
DOI: 10.1126/sciadv.aao3773

**This PDF file includes:**

# Supplementary Materials

## section S1. Magnetocaloric effect

By definition, the magnetic Grüneisen parameter $\Gamma_H = -\frac{\frac{\partial M}{\partial T}\big|_H}{C}$ can be determined from the ratio of the temperature-derivative of the magnetization $M$ and the specific heat $C$, both measured at fixed values of the magnetic field $H$. Alternative experimental methods to determine $\Gamma_H$ are described, e.g., in Refs. (36–38). Here, we chose to measure the isothermal entropy change $\frac{\partial S}{\partial H}\big|_T = \frac{\partial M}{\partial T}\big|_H$ in a continuous way while sweeping the magnetic field. The experimental setup consists of a standard thermal relaxation-time calorimeter where the sample is fixed to the sample platform using a small amount of Apiezon N grease. While sweeping the magnetic field, the sample temperature $T$ is kept at a constant difference $\Delta T$ above the bath temperature $T_0$ by adjusting the power $P$ applied to the sample heater at the platform, which is coupled by the thermal conductance $K$ to the heat bath (cf. fig. S1). Under isothermal conditions, the entropy change $dS$ is given by its field dependence

$$T\,dS = T\,\frac{\partial S}{\partial H}\bigg|_T dH = (P - K\,\Delta T)\,dt \tag{1}$$

which is balanced by a variation of the heating power $P$. For reversible processes

$$P_\gamma(H) = K\,\Delta T + \gamma\,T\,\frac{\partial S}{\partial H}\bigg|_T \tag{2}$$

where $\gamma = \frac{dH}{dt}$ denotes the magnetic-field sweep rate. As expected $P_\gamma(H)$ is antisymmetric with respect to the field-sweep direction, see fig. S1, and the isothermal magnetic-field dependence of the entropy is given by

$$\frac{\partial S}{\partial H}\bigg|_T = \frac{P_\gamma(H) - P_{-\gamma}(H)}{2\,|\gamma|\,T} \tag{3}$$

The magnetic-field dependent Grüneisen parameter $\Gamma_H$ is then obtained by additionally dividing by the heat capacity as a function of $H$, which was measured in a separate run in the same setup using the thermal relaxation time method.

## section S2. Deviations of C around 2.5 K

Around 2.5 K, the specific heat calculated for the Heisenberg model deviates by up to 10 % from the experimental data. These deviations cannot be explained by phonon or nuclear contributions because the bare magnetic contribution $C_{1\mathrm{D}}$ is already larger than the total measured specific heat. This experimental result was reproduced by measurements on different CuPzN crystals

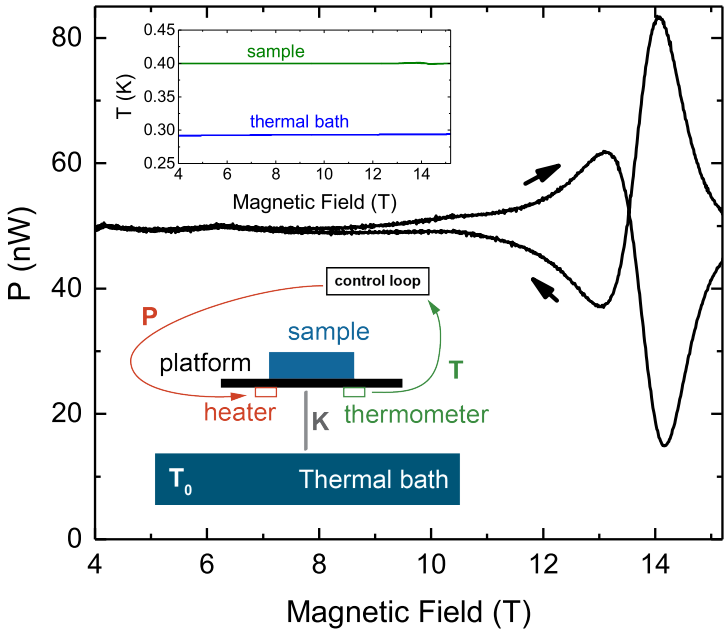


**fig. S1. Magnetocaloric effect measurement.** Raw data of the heating power P applied to the sample heater during a magnetic field sweep with increasing and decreasing magnetic field (indicated by arrows) at a rate of $\pm 0.2$ T/min, acquired with a setup as schematically shown in the main panel. While sweeping the field, the temperatures of the sample and of the thermal bath (shown in the inset) are constant within 1% at 0.29 and 0.4 K, respectively, which confirms the precise tuning of the temperature control loop.

from different growth procedures. Moreover, it has been independently obtained with our home-built low-temperature calorimeter and by using the specific heat option of the commercial PPMS system (Quantum Design). In order to fit the experimental data in this temperature range with the 1D Heisenberg model one would have to increase the exchange coupling $J$ by 10%, but this disagrees with the fits of all other (thermodynamic) measurements and would also decrease the overall agreement of the general $C(T, H)$ data.

## section S3. Nuclear contributions

Nuclear contributions can be identified in the specific heat data at low temperature $T \lesssim 0.5$ K. They arise from the nuclear spins ($I = 3/2$) of the copper atoms in the compound due to a finite splitting of energy levels by hyperfine interactions and their thermal occupation. Here, we restrict ourselves to interactions with the external magnetic field $\mu_0 H$ and with the hyperfine field arising from the spins of the surrounding unpaired electrons, which is proportional to the

magnetic moment $m_{1D}$ per spin of the Heisenberg chain. The nuclear free energy per atom is

$$\mathcal{F}_{\rm nuc} = -k_{\rm B}T \log \left[ \sum_{I=-3/2}^{I=3/2} e^{\frac{-g_N \mu_{\rm N} B_{\rm hf} I}{k_{\rm B} T}} \right] \tag{4}$$

with the natural abundance-averaged nuclear g factor $g_N \simeq 1.516$ of copper, the nuclear magnetic moment $\mu_{\rm N}$, and the effective total hyperfine field $B_{\rm hf} = \mu_0 H + A m_{1D}$. Note that the single adjustable parameter of Eq. (4) is $A$, which describes the coupling of the net magnetization to the hyperfine field. Within the temperature range of the present experiment $T \gg g_N \mu_N B_{\rm hf}/k_{\rm B}$ ($\approx 0.05\,{\rm K}$ for a typical value $B_{\rm hf} \approx 10^2\,{\rm T}$) only the high-temperature tail of a Schottky anomaly contributes to the molar specific heat,

$$C_{\rm nuc}/(N_{\rm A} k_{\rm B}) \approx B_{\rm hf}^2\, g_N^2\, \mu_N^2 I(I+1)/(3\, k_{\rm B}^2\, T^2) \tag{5}$$

Fitting our low-temperature data with the sum $C = C_{1D} + C_{\rm nuc}$ of the Heisenberg spin chain (see main text) and the nuclear contribution we obtain $A = 46\,{\rm T}\mu_{\rm B}^{-1}$, which is comparable to the values found for other transition metal systems (39). Apparently, the hyperfine field $B_{\rm hf}$ is mainly determined by the spin chain's magnetization, which is reflected in the nuclear heat capacity's strong resemblance to the magnetization (cf. Fig. 2(C,E) of the main text).

A sizable nuclear contribution is only found in the specific heat at 0.3 and 0.5 K. Nuclear contributions are neither seen in $\alpha$ and $\lambda$ nor in $m$ at any temperature. For $\alpha$ and $\lambda$, this results from negligibly small pressure dependencies of $\mathcal{F}_{\rm nuc}$ and for $m$ it is due to the smallness of $\mu_N \ll \mu_{\rm B}$. In case of the magnetocaloric effect the critical contribution

$$\Gamma_{H,1D} = \frac{\partial S/\partial H - \partial S_{\rm nuc}/\partial H}{C - C_{\rm nuc} - C_{\rm phon}} \tag{6}$$

actually differs from the directly measured total $\Gamma_H = \frac{\partial S/\partial H}{C}$. The only relevant difference, however, arises from the same nuclear contribution $C_{\rm nuc}$ to the heat capacity discussed above. In the relevant low-temperature range the phonon contribution $C_{\rm phon}$ can be safely neglected and also the nuclear contribution to the entropy change $\partial S_{\rm nuc}/\partial H$ turns out to be negligibly small (see dotted line in Fig. 2(F) of the main text).

# section S4. Quantum critical theory and corrections to scaling

In this section we review the quantum critical theory describing the field-induced quantum phase transition of the Heisenberg chain. Moreover, we discuss the leading corrections to scaling for the various thermodynamic quantities measured in our experiment. In particular, we address the observation that the deviations from the critical scaling curve is larger for the susceptibility

and the magnetostriction as compared to the specific heat and thermal expansion, see Fig. 3 of the main text. We show that this is a matter of numerical coefficients that are formally of order one but turn out to be larger for the former than for the latter two quantities.

## S4.1. Free energy per spin close to quantum criticality

The Bethe-Ansatz approach yields the free energy of the Heisenberg spin chain in terms of the non-linear integral equations (5) and (6) in the main manuscript. An asymptotic analysis of these equations provides the following expression for the free energy per spin close to quantum criticality (see Eq. (2) of the main text)

$$\mathcal{F} = \frac{J - 2g\mu_{\rm B}\mu_0 H}{4} + \frac{(k_{\rm B}T)^{3/2}}{\sqrt{J}} f_0\Big(\frac{g\mu_{\rm B}\mu_0(H-H_c)}{k_{\rm B}T}\Big) + \frac{(k_{\rm B}T)^2}{J} f_1\Big(\frac{g\mu_{\rm B}\mu_0(H-H_c)}{k_{\rm B}T}\Big) + \dots \tag{7}$$

where the functions $f_0$ and $f_1$ are given by

$$f_0(x) = -\frac{\sqrt{2}}{\pi}\int_0^\infty dy \log(1+e^{-y^2-x}), \qquad f_1(x) = -\frac{1}{2} f_0(x) f_0'(x) \tag{8}$$

with the derivative $f_0'(x) = \frac{df_0(x)}{dx}$. We mention that the authors of Ref. (22) use the standard thermodynamical Bethe ansatz formulation (13, 14) and truncate the infinite hierarchy of coupled equations to a manageable finite set. Our approach (15, 35) is based on a finite set of equations from the beginning. In the very low-temperature limit both formulations reduce to the same single non-linear integral equation. Therefore, up to the given order of Eq. (7) the low-temperature asymptotics presented here agrees with the result of Ref. (22), which also targets even higher-order corrections.

In the following, we explain that the leading terms of Eq. (7) have an intuitive interpretation and can be derived by elementary methods. Performing a standard Jordan-Wigner transformation for the spins, the Heisenberg Hamiltonian of Eq. (1) in the main text at $\Delta = 1$ can be written in the form

$$\mathcal{H} = \sum_i \left( -\frac{J}{2}\left(c_i^\dagger c_{i+1} + c_{i+1}^\dagger c_i\right) + J\left(n_{i+1} - \frac{1}{2}\right)\left(n_i - \frac{1}{2}\right) + g\mu_{\rm B}\mu_0 H\left(n_i - \frac{1}{2}\right)\right) \tag{9}$$

where $n_i = c_i^\dagger c_i$. In the field-polarized state at large $H$, the density of spinons described by the fermionic annihilation operator $c_i$ on site $i$ is dilute. The first term in Eq. (7) just corresponds to the energy of the field polarized ground state that is empty of spinons. The second term in Eq. (7) is recovered by the thermal excitation of non-interacting spinons. At low temperatures, spinons with energy $\varepsilon_k = -J\cos(ak) - (J - g\mu_{\rm B}\mu_0 H)$, where $a$ is the lattice constant, only

contribute here for small wavevectors $\varepsilon_k \approx \frac{J}{2}(ak)^2 - (2J - g\mu_\mathrm{B}\mu_0 H)$, which identifies the mass $m = \hbar^2/(Ja^2)$ and the chemical potential $\mu = g\mu_\mathrm{B}\mu_0 H_c - g\mu_\mathrm{B}\mu_0 H$ with the critical field $g\mu_\mathrm{B}\mu_0 H_c = 2J$. The integral in the $f_0$ function arises from the summation over momentum states after substituting $y = \lambda_T k$ with the thermal wavelength $\lambda_T = \frac{\hbar}{\sqrt{2mk_\mathrm{B}T}}$. This second term in Eq. (7) governs the low-energy asymptotics close to criticality.

Finally, the third term in Eq. (7) defines the leading correction to scaling and derives from the interaction $Jn_{i+1}n_i$ between spinons in Eq. (9). Up to a factor of $1/2$, it is already obtained by treating this interaction in first-order perturbation theory and taking the low-temperature limit. The product $f_0 f_0'$ in the definition of the $f_1$ function can be identified with a product of two momentum integrals whose integrands contain Fermi functions quantifying the occupation probability of spinons. For the $f_0$ function this becomes apparent after an integration by parts

$$f_0(x) = -\frac{\sqrt{2}}{\pi}\int_0^\infty dy \frac{2y^2}{1+e^{y^2+x}} \tag{10}$$

The additional factor $y^2$ in the integrand arises from the Pauli principle and reflects that two spinons cannot simultaneously occupy the same state. In order to obtain the correct numerical prefactor for the leading correction to scaling, however, one has to take into account the full two-spinon $T$-matrix, i.e., the whole series of ladder diagrams in the two-spinon sector must be summed up. The resulting $T$-matrix is given by $T(E) = J/(1 - J\Pi(E))$ with

$$\Pi(E) = a\int_{-\pi/a}^{\pi/a} \frac{dk'}{2\pi}\frac{2\sin^2(k'a)}{E - 2\varepsilon_{k'}} \tag{11}$$

In the low-temperature limit, we can approximate the on-shell energy $E$ by the energy of two spinons at zero wavevector, i.e., $E = \varepsilon_k + \varepsilon_{-k} \approx 2\varepsilon_0 = -2(2J - g\mu_\mathrm{B}\mu_0 H)$. The integral in Eq. (11) then simplifies to $\Pi = -1/J$ and the on-shell $T$-matrix becomes $T = J/2$ yielding the additional factor of $1/2$. The repeated scattering between two spinons thus reduces by half the correction to scaling.

## S4.2. Critical thermodynamics

The theoretical prediction for the quantum critical thermodynamics of CuPzN is shown for temperatures $T = 2$ K and $T = 0.25$ K in fig. S2 that compares the full Bethe-Ansatz result (dashed lines) with the critical scaling curve (black solid line) deriving only from the second term in Eq. (7) and with the curves that include the leading correction to scaling deriving from the third term in Eq. (7) (red and blue solid lines).

The leading correction to scaling, i.e., the third term in Eq. (7) is systematically smaller than the second term by a factor of $\sqrt{k_\mathrm{B}T/J}$. Scaling close to criticality is only expected in

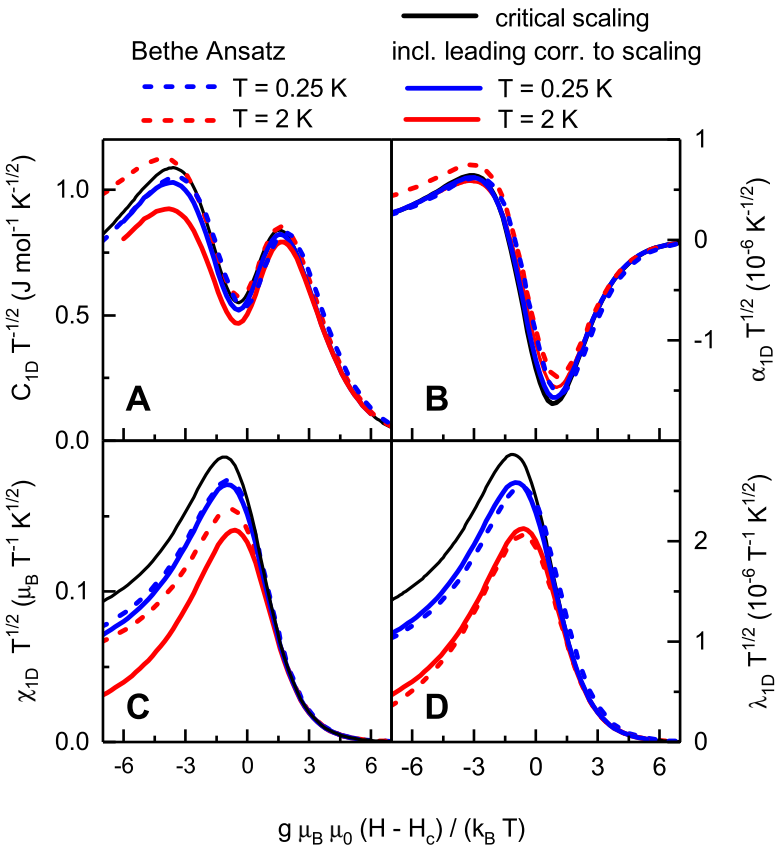


**fig. S2. Theoretical prediction for the scaling of quantum critical thermodynamics in CuPzN.** The dashed lines show the exact Bethe-Ansatz result describing the experimental data as shown in Fig. 3 of the main text. The solid black line is the critical scaling asymptotics deriving from the second term in Eq. (7) and the red and blue solid lines include the leading correction to scaling, i.e., also the third term in Eq. (7). The latter is sufficient for a reasonable description of the full Bethe-Ansatz result at $T = 0.25$ K but fails at $T = 2$ K, where further sub-leading corrections are important.

the limit $\sqrt{k_{\rm B}T/J} \ll 1$ when the correction to scaling is negligible. For CuPzN $J/k_{\rm B} = 10.6$ K so that $\sqrt{k_{\rm B}T/J} \approx 43\%$ at a temperature $T = 2$ K and still $\sqrt{k_{\rm B}T/J} \approx 15\%$ at $T = 0.25$ K, which is the lowest temperature where we have performed measurements. As a result, the scaling corrections are in general expected to be sizeable in our experimental data. This explains the deviations from the universal scaling curve observed for the susceptibility and the magnetostriction in panel (C) and (D), respectively, of fig. S2 as well as Fig. 3 of the main text. As we will show in the following, small numerical coefficients further suppress the leading correction to scaling in the other thermodynamic quantities explaining the good

scaling collapse of the specific heat, thermal expansion, magnetocaloric effect and Grüneisen parameter, see Fig. 3 of the main text.

### S4.2a. Specific heat

The molar specific heat is defined as $C = -N_\mathrm{A} T \frac{\partial^2 \mathcal{F}}{\partial T^2}$ with the Avogadro constant $N_\mathrm{A}$. The critical scaling part and the leading scaling correction can be cast in the scaling form

$$C_0 = N_\mathrm{A} k_\mathrm{B} \sqrt{\frac{k_\mathrm{B}T}{J}} \Phi_0^C \Big( \frac{g\mu_\mathrm{B}\mu_0(H-H_c)}{k_\mathrm{B}T} \Big), \quad C_1 = N_\mathrm{A} k_\mathrm{B} \frac{k_\mathrm{B}T}{J} \Phi_1^C \Big( \frac{g\mu_\mathrm{B}\mu_0(H-H_c)}{k_\mathrm{B}T} \Big) \quad (12)$$

where the two scaling functions, $\Phi_0^C$ and $\Phi_1^C$, are straightforwardly related to $f_0$ and $f_1$ in Eq. (7). These functions and their ratio are shown in fig. S3 (A) and (B), respectively. The relative correction $C_1/C_0 = \sqrt{\frac{k_\mathrm{B}T}{J}} \Phi_1^C/\Phi_0^C$ is most pronounced at $x \approx -2$ where $\Phi_1^C/\Phi_0^C \approx -0.4$. At $T = 0.3$ K relative corrections $C_1/C_0$ of at most $7\%$ are expected, which are too small to be identified clearly in the experimental data.

### S4.2b. Susceptibility

For the magnetic susceptibility, defined by $\chi = -\frac{\partial^2 \mathcal{F}}{\partial(\mu_0 H)^2}$, the critical part and the leading scaling correction assume the scaling form

$$\chi_0 = \frac{(g\mu_\mathrm{B})^2}{J} \sqrt{\frac{J}{k_\mathrm{B}T}} \Phi_0^\chi \Big( \frac{g\mu_\mathrm{B}\mu_0(H-H_c)}{k_\mathrm{B}T} \Big), \quad \chi_1 = \frac{(g\mu_\mathrm{B})^2}{J} \Phi_1^\chi \Big( \frac{g\mu_\mathrm{B}\mu_0(H-H_c)}{k_\mathrm{B}T} \Big) \quad (13)$$

The scaling functions $\Phi_0^\chi$ and $\Phi_1^\chi$, resulting again from $f_0$ and $f_1$ of Eq. (7), respectively, are shown in fig. S3 (C) and (D) together with their ratio $\Phi_1^\chi/\Phi_0^\chi$. This ratio is negative and monotonically decreases with decreasing argument $x$ and already exceeds $-1$ at $x \approx -3.5$. Thus, the leading corrections to scaling for $\chi$ are much larger than for the specific heat. At $T = 0.3$ K and $x \approx -5$, the relative correction $\chi_1/\chi_0$ reaches about $-21\%$, which explains the relatively large deviations of the experimental susceptibility data from the critical scaling curve $\chi_0$ for $H < H_c$, see Fig. 3 of the main text.

### S4.2c. Thermal expansion

The linear thermal expansion describes the change of length $L$ upon a change of the temperature, $\alpha = \frac{1}{L}\frac{\partial L}{\partial T} = \frac{1}{V_S}\frac{\partial^2 \mathcal{F}}{\partial p \partial T}$ where $p$ is the uniaxial pressure and $V_S$ is the volume per spin. We assume that the pressure dependence arises from a magnetoelastic coupling that yields a weakly pressure dependent exchange $J(p)$. The free energy (7) depends on $J$ via the critical field $H_c$ in the arguments of the functions $f_0$ and $f_1$ as well as via their prefactors. The critical scaling

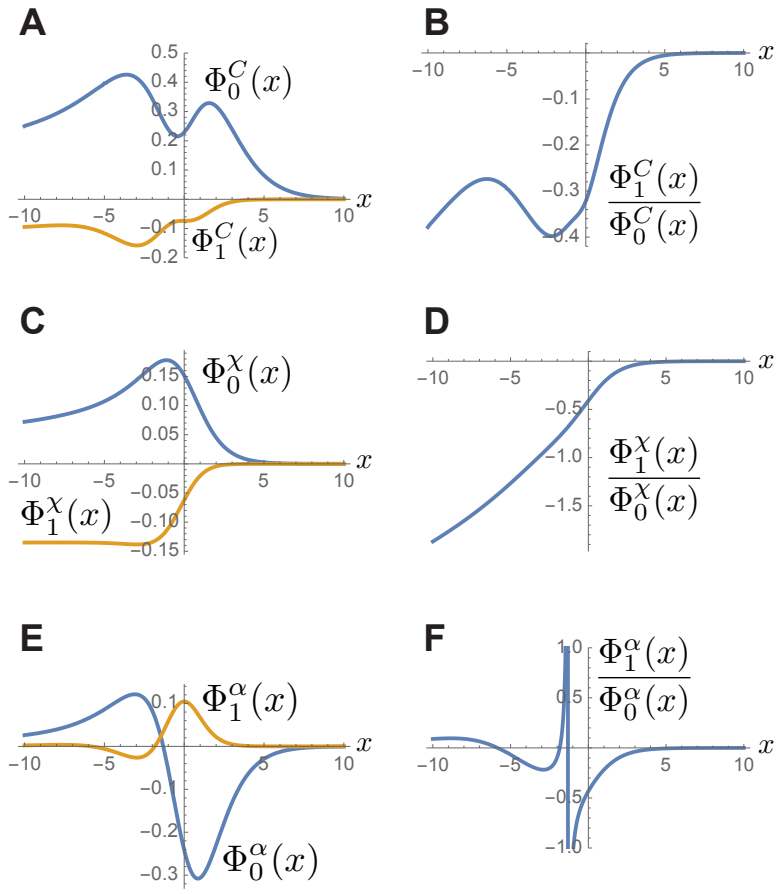


**fig. S3. Deviations from critical scaling.** Scaling functions for the critical contribution, $\Phi_0$, and the leading correction to scaling, $\Phi_1$, as well as their ratio $\Phi_1/\Phi_0$ for the specific heat $C$ (**A**, **B**), the susceptibility $\chi$ (**C**, **D**), and the thermal expansion $\alpha$ (**E**, **F**). Whereas the ratio $\Phi_1^\chi/\Phi_0^\chi$ in panel (**D**) reaches absolute values exceeding $1.5$, the corresponding ratios in panel (**B**) and (**F**) are relatively small explaining the good scaling collapse of the specific heat and thermal expansion observed in Fig. 3 of the main text.

contribution $\alpha_0$ to the thermal expansion as well as the leading correction to scaling $\alpha_1$ are both attributed to the pressure dependence of $H_c$, respectively. The pressure dependences of their prefactors only give rise to further, subleading corrections to scaling. Both quantities, $\alpha_0$ and $\alpha_1$, can again be cast in the scaling form

$$\alpha_0 = \frac{k_\mathrm{B}}{JV_S}\frac{\partial J}{\partial p}\sqrt{\frac{J}{k_\mathrm{B}T}}\Phi_0^\alpha\Big(\frac{g\mu_\mathrm{B}\mu_0(H-H_c)}{k_\mathrm{B}T}\Big), \quad \alpha_1 = \frac{k_\mathrm{B}}{JV_S}\frac{\partial J}{\partial p}\Phi_1^\alpha\Big(\frac{g\mu_\mathrm{B}\mu_0(H-H_c)}{k_\mathrm{B}T}\Big) \tag{14}$$

The scaling functions $\Phi_0^\alpha$ and $\Phi_1^\alpha$ again result from $f_0$ and $f_1$, respectively, and are shown together with their ratio $\Phi_1^\alpha/\Phi_0^\alpha$ in fig. S3 (E) and (F). Except close to the sign change of $\Phi_0^\alpha$,

the absolute value of $\Phi_1^\alpha/\Phi_0^\alpha$ is smaller than $0.2$. Thus, the leading corrections to scaling for $\alpha$ are of similar magnitude as those of the specific heat.

### S4.2d. Magnetostriction

Finally, we discuss the magnetostriction $\lambda = \frac{1}{L}\frac{\partial L}{\partial(\mu_0 H)} = \frac{1}{V_S}\frac{\partial^2 \mathcal{F}}{\partial p \partial(\mu_0 H)}$. In analogy to the thermal expansion, the critical contribution $\lambda_0$ and the leading correction $\lambda_1$ derive from the pressure dependence of $H_c$ in the arguments of the functions $f_0$ and $f_1$ in Eq. (7), respectively. At this order, both quantities can be related to the corresponding ones of the susceptibility, that is: $\lambda_0 = \frac{1}{V_S}\frac{2}{g\mu_B}\frac{\partial J}{\partial p}\chi_0$ and $\lambda_1 = \frac{1}{V_S}\frac{2}{g\mu_B}\frac{\partial J}{\partial p}\chi_1$. From the discussion of the susceptibility we can thus conclude that the corrections to scaling are relatively large for the magnetostriction at $H < H_c$.